J. Fluid Mech. (1980), *vol.* 97, *part* 2, *pp.* 257–277
Printed in Great Britain

Infinite Prandtl number thermal convection in a spherical shell

By ABDELFATTAH ZEBIB,

Department of Mechanical, Industrial and Aerospace Engineering, College of Engineering, Rutgers University, Piscataway, New Jersey 08854

GERALD SCHUBERT

Department of Earth and Space Sciences, University of California, Los Angeles, California 90024

AND JOE M. STRAUS

Space Sciences Laboratory, The Aerospace Corporation, P.O. Box 92957, Los Angeles, California 90009

(Received 5 March 1979)

A Galerkin method is used to calculate the finite amplitude, steady, axisymmetric convective motions of an infinite Prandtl number, Boussinesq fluid in a spherical shell. Convection is driven by a temperature difference imposed across the stress-free, isothermal boundaries of the shell. The radial gravitational field is spherically symmetric and the local acceleration of gravity is directly proportional to radial position in the shell. Only the case of a shell whose outer radius is twice its inner radius is considered. Two distinct classes of axisymmetric steady states are possible. The temperature and radial velocity fields of solutions we refer to as 'even' are symmetric about an equatorial plane, while the latitudinal velocity is antisymmetric about this plane; solutions we refer to as 'general' do not possess any symmetry properties about the equatorial plane. The characteristics of these solutions, i.e. the isotherms, streamlines, spherically averaged temperature profiles, Nusselt numbers, etc., are given for Rayleigh numbers Ra as high as about 10 times critical for the even solutions and 3 times critical for the general solutions. Linear stability analyses of the nonlinear steady states show that the general solutions are the preferred form of axisymmetric convection when Ra is less than about 4 times critical. Furthermore, while the preferred motion at the onset of convection is non-axisymmetric, axisymmetric convection is stable when Ra exceeds about 1·3 times the critical value.

1. Introduction

Solid state mantle convection is now recognized as the most efficient means of transferring heat from the earth's interior to its surface (Tozer 1967; Turcotte & Oxburgh 1972; Oxburgh & Turcotte 1978; Richter 1978; Schubert 1979). To determine how this heat transport occurs, we must understand the nature of thermal convection in infinite Prandtl number fluids (the Prandtl number of the earth's mantle, i.e. the

0022–1120/80/4404–8490 $02.00

ratio of its kinematic viscosity to its thermal diffusivity is about 10^{23}). Furthermore, while convection in the uppermost mantle may be modelled in a planar geometry, a spherical geometry in required to properly describe whole mantle convection. Thus, the major objective of the present paper is to determine the characteristics of infinite Prandtl number thermal convection in spherical shells. We need not be concerned with effects of rotation since the Coriolis force is negligible in the highly viscous mantle (the Taylor number, which measures the ratio of Coriolis forces to viscous forces is $O(10^{-16})$ for whole mantle convection). Basic fluid dynamical calculations of finite-amplitude thermal convection in spherical geometry have been carried out by Hsui, Turcotte & Torrance (1972) and Young (1974). Numerical models of the thermal states of planetary interiors based on computations of axisymmetric convection in spheres and spherical shells have been constructed by Turcotte *et al.* (1972), Young & Schubert (1974), Cassen & Young (1975), Schubert & Young (1976) and Schubert, Young & Cassen (1977).

Steady state, nonlinear convection in spherical shells may be realized in either of two forms – axisymmetric motion, which is analogous to two-dimensional rolls in a plane fluid layer heated from below, or non-axisymmetric motion, which is analogous to three-dimensional convection in a plane fluid layer. Each of these two forms of convection may exist as motions which either exhibit symmetry properties about an 'equatorial' plane or motions which do not. Solutions which have equatorially symmetric temperature and radial velocity fields and an equatorially antisymmetric latitudinal velocity field are referred to as 'even'. 'General' solutions are those not possessing these symmetry properties. Young's (1974) computations of axisymmetric and fully three-dimensional convection in spherical shells were restricted to the even flows. Busse's (1975) analysis of the preferred motion at the onset of convection is able to discriminate between axisymmetric and fully three-dimensional patterns only for the even solutions.

In this paper we use a Galerkin technique to calculate the steady state, axisymmetric, nonlinear, convective motions in an infinite Prandtl number, Boussinesq fluid in a relatively thick spherical shell heated from below. We will carry out a reasonably complete study of the properties of the even and general axisymmetric steady states for a range of modestly supercritical Rayleigh numbers. In addition, we will perform stability analyses to decide which form of axisymmetric steady convection is the preferred one and whether the axisymmetric steady flows are unstable to azimuthal perturbations.

2. Mathematical formulation

We consider an infinite Prandtl number Pr ($Pr = \nu/\kappa$ where ν is the kinematic viscosity and κ is the thermal diffusivity) Boussinesq fluid in a spherical shell. The validity of the Boussinesq approximation in mantle convection has been discussed by Schubert (1979) and others referenced therein. The stress-free, isothermal boundaries of radii R_1, R_2 ($R_2 > R_1$) are maintained at temperatures T_1, T_2 ($T_1 > T_2$), respectively. The density is assumed constant except for the buoyancy term and all other thermodynamic and transport properties of the fluid are also assumed constant. The fluid is devoid of internal heat sources and the local acceleration of gravity is directly proportional to radial position in the shell, as is appropriate to a homogeneous fluid sphere of

density ρ. The non-dimensional equations which describe the motion of the fluid are

$$\nabla.\mathbf{v} = 0, \tag{2.1}$$

$$(1-\eta)\,Ra\nabla\times(\Theta\mathbf{r})+\nabla\times\nabla^2\mathbf{v} = 0, \tag{2.2}$$

$$\frac{\partial\Theta}{\partial t}+(\mathbf{v}.\nabla)(\Theta_c+\Theta) = \nabla^2\Theta. \tag{2.3}$$

In (2.1)–(2.3), $\mathbf{r}$, the velocity $\mathbf{v}$, time t, and temperature have been assumed dimensionless with respect to $d = R_2-R_1$, κ/d, d^2/κ and $\Delta T = T_1-T_2$, respectively. $\Theta(\mathbf{r},t)$ is the temperature deviation from the basic state conduction profile $\Theta_c(r)$,

$$\Theta_c = \frac{r_1 r_2}{r}-r_1, \tag{2.4}$$

$$r_1 = \frac{R_1}{d} = \frac{\eta}{1-\eta}, \quad r_2 = \frac{R_2}{d} = \frac{1}{1-\eta}, \tag{2.5}$$

where $\eta = R_1/R_2$ is the shell thickness parameter. The Rayleigh number Ra is given by

$$Ra = \frac{\alpha g_0 \Delta T d^3}{\nu\kappa}, \tag{2.6}$$

where α is the coefficient of thermal expansion and g_0 is the value of the acceleration of gravity at the outer radius. Equation (2.2) is the curl of the momentum equation, while (2.1) and (2.3) are the standard continuity and temperature equations. The boundary conditions for (2.1)–(2.3) are

$$\Theta = v_r = \frac{\partial^2}{\partial r^2}(rv_r) = 0 \quad \text{at} \quad r = r_1, r_2, \tag{2.7}$$

where v_r is the radial velocity component (Chandrasekhar 1961).

The solenoidal velocity field can be written in terms of poloidal and toroidal functions which automatically satisfy the continuity equation (Chandrasekhar 1961). However, one can show that the velocity field is purely poloidal in the infinite Prandtl number limit (see appendix and compare with a similar result of Busse 1967 for planar geometry). Thus, we introduce the poloidal function $\Phi(\mathbf{r},t)$ in terms of which $\mathbf{v}$ is given by

$$\mathbf{v} = \left(\frac{1}{r^2}L^2\Phi, \frac{1}{r}\frac{\partial^2\Phi}{\partial r\partial\theta}, \frac{1}{r\sin\theta}\frac{\partial^2\Phi}{\partial r\partial\phi}\right), \tag{2.8}$$

where (r,θ,ϕ) are spherical co-ordinates and the differential operator L^2 is

$$L^2 = -\frac{1}{\sin\theta}\frac{\partial}{\partial\theta}\left(\sin\theta\frac{\partial}{\partial\theta}\right)-\frac{1}{\sin^2\theta}\frac{\partial^2}{\partial\phi^2} \tag{2.9}$$

(Chandrasekhar 1961). The linear 'momentum' equation (2.2) can be written in terms of Φ as

$$\nabla^4\left(\frac{1}{r}L^2\Phi\right) = (1-\eta)\,RaL^2\Theta \tag{2.10}$$

(Chandrasekhar 1961).

We are interested in constructing axisymmetric steady convective solutions and testing their stability to non-axisymmetric perturbations. There exists a stream function Ψ for an axisymmetric velocity field in terms of which

$$\mathbf{v} = \left(\frac{1}{r^2 \sin\theta}\frac{\partial \Psi}{\partial \theta}, \frac{-1}{r\sin\theta}\frac{\partial \Psi}{\partial r}, 0\right). \tag{2.11}$$

By comparing (2.11) and (2.8) in the case $\partial\Phi/\partial\phi = 0$ we find

$$\Psi = -\sin\theta\, \partial\Phi/\partial\theta. \tag{2.12}$$

We will use the Galerkin method to find the axisymmetric solutions to the basic equations and boundary conditions. Accordingly, we expand Θ and Φ in terms of Legendre polynomials $P_l(\cos\theta)$ and radial functions as follows

$$\Theta = \sum_{l=0}^{\infty}\sum_{j=1}^{\infty} \tau_{lj}(t)\sqrt{2}\sin\lambda_j(r-r_1)\, P_l(\cos\theta), \tag{2.13}$$

$$\Phi = (1-\eta)\, Ra \sum_{l=0}^{\infty}\sum_{j=1}^{\infty} \tau_{lj}(t)\, r f_{lj}(r)\, P_l(\cos\theta), \tag{2.14}$$

where $\lambda_j = j\pi$ and

$$\int_{-1}^{1} P_l(\mu)\, P_m(\mu)\, d\mu = \delta_{lm}. \tag{2.15}$$

The radial functions for Θ are chosen in a straightforward manner; the trigonometric functions $\sin\lambda_j(r-r_1)$ automatically satisfy the boundary conditions (2.7) on Θ. The functions $f_{lj}(r)$ for the poloidal velocity potential are not immediately obvious. They can be chosen so that (2.13) and (2.14) are exact solutions of the 'momentum' equation which automatically satisfy the boundary conditions (2.7) on v_r. Upon substituting (2.13) and (2.14) into (2.10) one obtains

$$D_l^2(f_{lj}) = \left(\frac{d^2}{dr^2} + \frac{2}{r}\frac{d}{dr} - \frac{l(l+1)}{r^2}\right)^2 f_{lj} = \sqrt{2}\sin\lambda_j(r-r_1). \tag{2.16}$$

The boundary conditions on v_r when expressed in terms of $f_{lj}(r)$ are

$$f_{lj} = \frac{d^2 f_{lj}}{dr^2} = 0 \quad \text{at} \quad r = r_1, r_2. \tag{2.17}$$

The functions $f_{lj}(r)$ are numerically constructed to satisfy (2.16) and (2.17).

The initial value problem for the expansion coefficients $\tau_{lk}(t)$ is formulated by substituting (2.13) and (2.14) into the temperature equation (2.3), using (2.8) to calculate $\mathbf{v}$ from Φ, multiplying by $\sin k\pi(r-r_1)\, P_l(\cos\theta)$ and integrating over the fluid region. The procedure eventually leads to

$$\frac{d}{dt}\tau_{lk} = \sum_{j=1}^{\infty} L_{ljk}\tau_{lj} + \sum_{n,m=0}^{\infty}\sum_{i,j=1}^{\infty} N_{nmijlk}\tau_{ni}\tau_{mj}, \tag{2.18}$$

where

$$L_{ljk} = -(1-\eta)\, Ra\, l(l+1)\, A_{ljk} + B_{ljk}, \tag{2.19}$$

$$A_{ljk} = \sqrt{2}\int_{r_1}^{r_2} \sin\lambda_k(r-r_1)\frac{f_{lj}}{r}\left(\frac{-r_1 r_2}{r^2}\right) dr, \tag{2.20}$$

$$B_{ljk} = 2\int_{r_1}^{r_2} \sin\lambda_k(r-r_1)\, D_j\{\sin\lambda_j(r-r_1)\} dr, \tag{2.21}$$

$$N_{nmijlk} = -(1-\eta)\,Ra\{C_{nijk}\,n(n+1) + D_{nijk}\,a_{nml}\}c_{nml}, \tag{2.22}$$

$$C_{nijk} = \lambda_j \int_{r_1}^{r_2} \frac{f_{ni}}{r}\{\sin[(\lambda_k+\lambda_j)(r-r_1)] + \sin[(\lambda_k-\lambda_j)(r-r_1)]\}dr, \tag{2.23}$$

$$D_{nijk} = \int_{r_1}^{r_2} \frac{d}{dr}(rf_{ni})\{\cos[(\lambda_k-\lambda_j)(r-r_1)] - \cos[(\lambda_k+\lambda_j)(r-r_1)]\}\frac{dr}{r^2}, \tag{2.24}$$

$$a_{nml} = \tfrac{1}{2}\{n(n+1) + m(m+1) - l(l+1)\}, \tag{2.25}$$

$$c_{nml} = \int_{-1}^{+1} P_n(\mu)\,P_m(\mu)\,P_l(\mu)\,d\mu. \tag{2.26}$$

It is important to realize that $c_{nml} = 0$ if $n+m+l$ is odd. Thus, N_{nmijlk} is zero for $n+m+l$ odd. If l is odd, it is clear from (2.18) that the nonlinear term vanishes if $n+m$ is even. Thus, if initial conditions are such that all τ_{lk} are zero for l odd, then τ_{lk} for l odd remains zero for all t. In other words, if an initial motion contains only even Legendre polynomials, it will remain equatorially symmetric with time (Young 1974).

3. Numerical procedure

The infinite sums in (2.18) must of course be replaced by finite ones. We take l, m, and n as large as N_θ and i, j, k as large as N_r. Convergence of the finite series representations is verified by increasing N_θ and N_r until pertinent characteristics of the solutions become sufficiently insensitive to the truncation. The sensitivity of the solutions to the values of N_θ and N_r will be made clear when we present our results in subsequent sections.

The functions f_{lj} were produced by combining the homogeneous solutions of (2.16) with numerically determined particular solutions of (2.16) so as to satisfy the boundary conditions (2.17). An integration step of 0·001 in r was used in calculating the particular solutions. The integrals in (2.20), (2.21), (2.23) and (2.24) were evaluated by the trapezoidal method, while those in (2.26) were computed using Bode's five points rule (Davis & Polonsky 1964). A data set incorporating all the relevant integrals was produced for $l \leqslant 14$ and $j \leqslant 10$.

The critical Rayleigh numbers $Ra_{\rm cr}$ for the onset of convection can be determined by setting the nonlinear terms in (2.18) to zero. The growth rates of perturbations, for each value of l, are then given by the eigenvalues of L_{ljk}. We found these eigenvalues to be real (exchange of stabilities), so that the critical Rayleigh number $Ra_{\rm cr}$ for each l corresponds to a zero eigenvalue. Our results, for $\eta = 0{\cdot}5$ and $N_r = 5$, are given in table 1. As shown in the table, they are in excellent agreement with Chandrasekhar's (1961) calculations.

For $Ra > Ra_{\rm cr}$, (2.18) can be integrated with arbitrary values of $\tau_{lk}(0)$ until a steady state with $\tau_{lk} = \bar{\tau}_{lk}$ is reached. When an explicit scheme is used, time steps of $O(10^{-5})$ are required to avoid numerical instability. Hence, we develop a fully-implicit scheme of integration. A Newton–Raphson method can also be used to find $\bar{\tau}_{lk}$ provided one has a good initial guess. This, of course, would be available if one had already established a steady state for an Ra not far from the one under consideration (cf. Clever & Busse 1974). The implicit scheme of integration was used to find the steady solutions only for Ra slightly larger than $Ra_{\rm cr}$. These solutions were then used as initial guesses

l	$Ra_{cr}(N_r = 5)$	Ra_{cr} (Chandrasekhar's 1961 2nd approximation)	Ra_{cr} (Chandrasekhar's 1961 3rd approximation)
1	2086·0	2100·0	2090·0
2	1095·5	1102·5	—
3	978·5	985·0	—
4	1109·5	1117·5	—
5	1410·0	1418·75	1412·5

TABLE 1. Critical Rayleigh numbers for the onset of convection in a spherical shell heated from below with $\eta = 0{\cdot}5$.

for the Newton–Raphson scheme at larger values of Ra. In the Newton–Raphson procedure, a steady state was assumed to be attained when

$$\left| \frac{\tau_{lk}^{(n+1)} - \tau_{lk}^{(n)}}{\tau_{lk}^{(n+1)}} \right| < 10^{-6},$$

where n is the iteration index. On the average, about 5 iterations were required to obtain a steady state. All computations were done on an IBM 370/168. CPU time requirements were 9 seconds per iteration with 64 expansion coefficients, and 42 seconds per iteration with 104 expansion coefficients.

4. Characteristics of the axisymmetric steady states

All the numerical results reported in this paper are for a relatively thick shell with $\eta = 0{\cdot}5$. For the Rayleigh numbers considered here, we have found that there generally exist two possible steady, axisymmetric solutions for each Ra. One subset of solutions, which we call 'even' is characterized by $\tau_{lk} \equiv 0$ for odd l. These solutions have equatorially symmetric temperature and radial velocity fields and an equatorially antisymmetric latitudinal velocity field. The second subset, which we refer to as 'general' solutions, includes non-zero values of τ_{lk} for both even and odd values of l. The general solutions have no special symmetry characteristics about the equator.

The heat transported by a convective flow is one important characteristic of the motion. It can be most readily evaluated at one of the boundaries where all the heat is transferred conductively. The heat flux averaged over the inner boundary $\langle q_i \rangle$ (the brackets on a quantity will denote an average over a spherical surface) is

$$\langle q_i \rangle = \frac{-k\Delta T}{d} \left(\frac{\partial \Theta_c}{\partial r} + \left\langle \frac{\partial \Theta}{\partial r} \right\rangle \right)_{r_1} \tag{4.1}$$

A similar expression holds for the average heat flux at the outer boundary $\langle q_o \rangle$. Conservation of energy requires $r_1^2 \langle q_i \rangle = r_2^2 \langle q_o \rangle$. For the basic conduction solution, we find from (2.4) that

$$q_c = \frac{-k\Delta T}{d} \frac{\partial \Theta_c}{\partial r} = \frac{k\Delta T}{d} \frac{r_1 r_2}{r^2}. \tag{4.2}$$

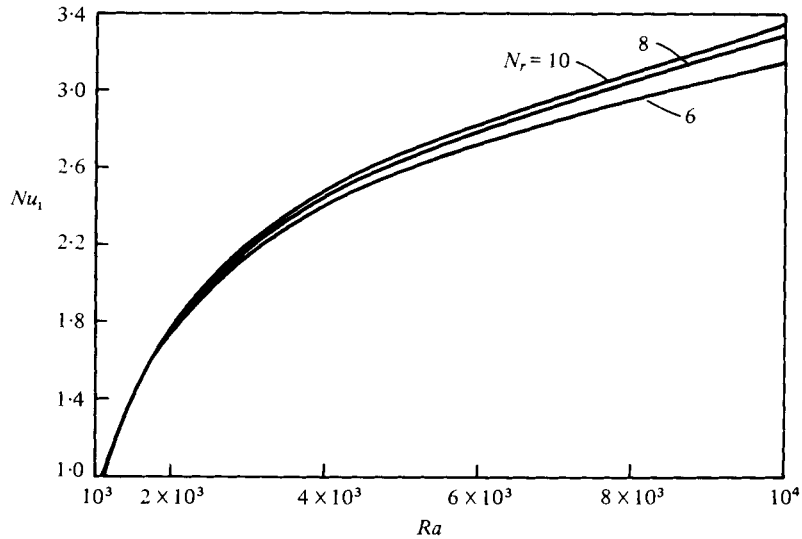

FIGURE 1. The Nusselt number at the inner shell boundary Nu_1 *vs.* Ra for the even, axisymmetric steady solutions with $N_\theta = 14$.

The Nusselt number Nu is the ratio of the heat transported by the convective state to the heat flux in the basic conductive state

$$Nu_{1,0} \equiv \frac{\langle q_{1\,0}\rangle}{(q_c)_{r_1,r_2}} = 1 - \left\{\frac{r^2}{r_1 r_2}\left\langle\frac{\partial\Theta}{\partial r}\right\rangle\right\}_{r_1,r_2}. \tag{4.3}$$

Conservation of energy requires $Nu_1 = Nu_0$. For the axisymmeric steady states, (2.13) and (4.3) gives

$$Nu_1 = 1 - \pi\eta \sum_{j=1}^{\infty} j\bar{\tau}_{0j}, \tag{4.4}$$

$$Nu_0 = 1 - \frac{\pi}{\eta}\sum_{j=1}^{\infty}(-1)^j j\bar{\tau}_{0j}. \tag{4.5}$$

Because the infinite series in (4.4) and (4.5) are truncated at $j = N_r$ in the numerical computations, the calculated values of Nu_1 and Nu_0 will not necessarily be equal. A comparison of these quantities provides a quantitative measure of the accuracy of a solution.

4.1. *Heat transfer for the even solutions*

According to table 1, even solutions exist for $Ra > 1095$; the minimum Ra_{cr} for the even modes occurs for $l = 2$. Figure 1 shows the variation of Nu_1 with Ra for $N_\theta = 14$ (8 Legendre polynomials) and $N_r = 6$, 8 and 10. At $Ra = 10^4$, the change in Nu_1 when N_r is increased from 9 to 10 is less than 1 %. The value $N_r = 8$ is generally adequate for computations with $Ra \lesssim 10^4$. Figure 2 shows the $Nu_1 - Ra$ relationship for $N_r = 8$ and $N_\theta = 10$, 12 and 14. The change in Nu_1 when N_θ is increased from 12 to 14 is less than 1 % at $Ra = 4000$ and about 2 % at $Ra = 5000$. The inflexion in the curve for $N_\theta = 12$, which occurs at $Ra \approx 6780$, is similar to one reported by Young (1974). However, the inflexion seems to be dependent on the resolution since it does not appear in the curves for $N_\theta = 10$ and 14. Thus, it has no real physical significance.

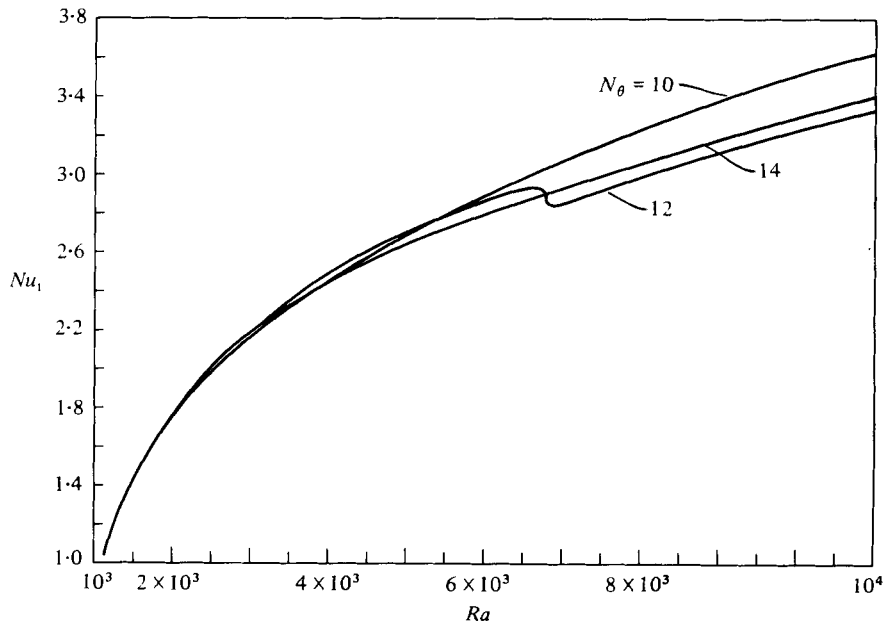

FIGURE 2. Same as figure 1 with $N_r = 8$.

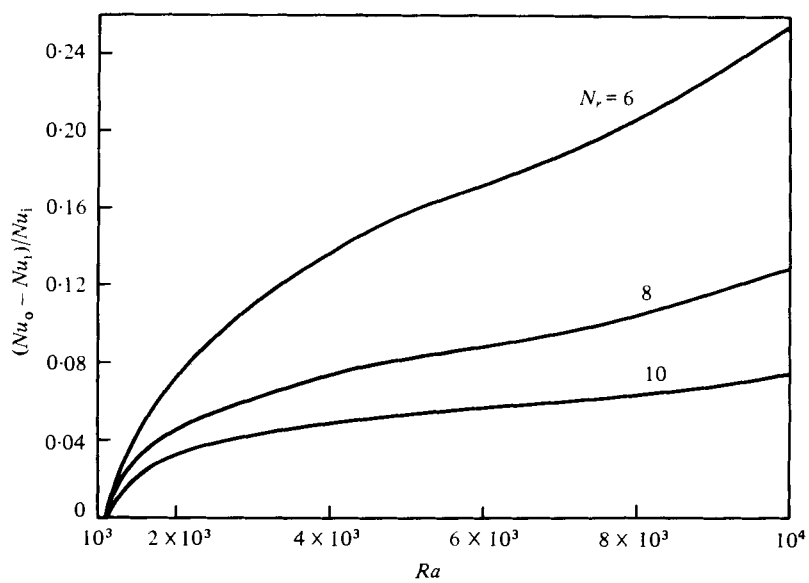

FIGURE 3. The fractional difference between the Nusselt numbers evaluated at the inner and outer shell radii, Nu_i and Nu_o, respectively, as a function of Rayleigh number Ra for $N_\theta = 14$.

Figures 3 and 4 show $(Nu_o - Nu_i)/Nu_i$ *vs.* Ra. In figure 3, $N_\theta = 14$ and $N_r = 6$, 8, and 10, while in figure 4, $N_r = 8$ and $N_\theta = 10$, 12 and 14. For the most accurate solution, $N_r = 10$, $N_\theta = 14$, it can be seen from figure 3 that the numerical error in the energy balance is about 7·5% at $Ra = 10^4$. Greater accuracy can be obtained by further increasing N_r and N_θ.

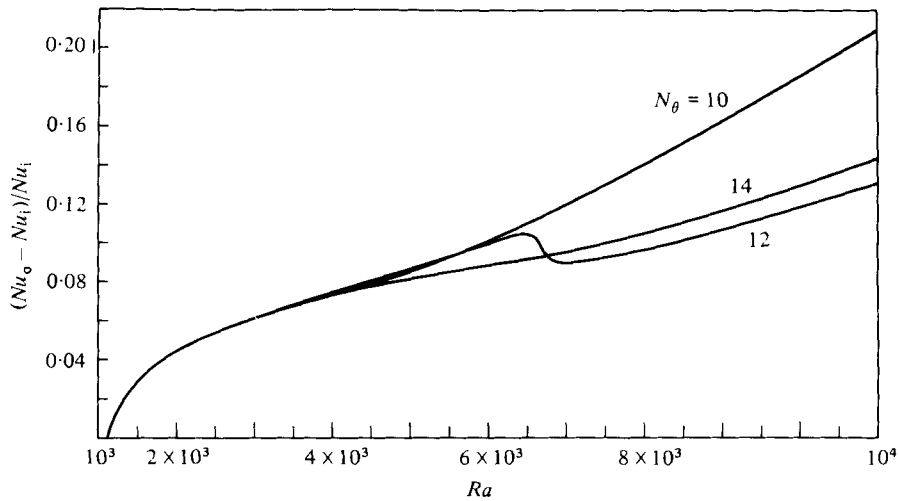

FIGURE 4. Same as figure 3 with $N_r = 8$.

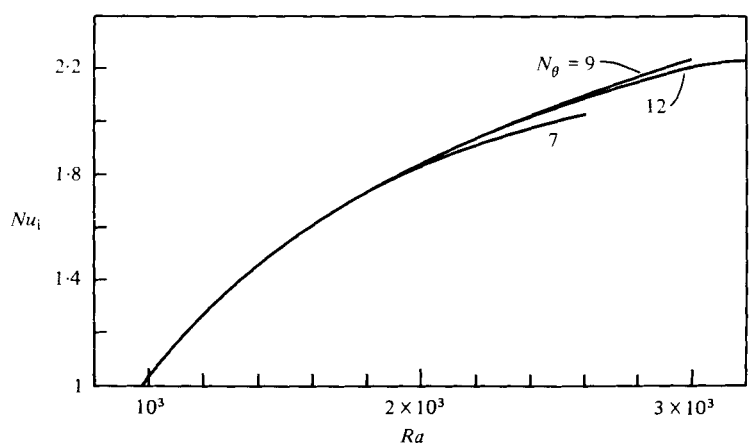

FIGURE 5. Same as figure 2 for the general, axisymmetric, steady solutions.

4.2. *Heat transfer for the general solutions*

General solutions are possible for $Ra > 978$; the minimum Ra_{cr} for all l occurs for $l = 3$ (see table 1). Figure 5 shows Nu_i *vs.* Ra for $N_r = 8$ and $N_\theta = 7$, 9 and 12. The largest Ra at which a steady state was obtained with our numerical approach depended on the resolution. We were able to determine solutions for $Ra \leqslant 2600$ with $N_\theta = 7$, for $Ra \leqslant 3000$ with $N_\theta = 9$ and for $Ra \leqslant 3200$ with $N_\theta = 12$. With $N_r = 8$ and $N_\theta = 12$, the general solutions require 104 expansion coefficients. For larger values of N_r and N_θ, the computations would become rather expensive. The error in the energy balance $(Nu_o - Nu_i)/Nu_i$ is less than 7 % for $978 < Ra < 3200$. The general solutions transport slightly more heat than do the even solutions in this range of Ra.

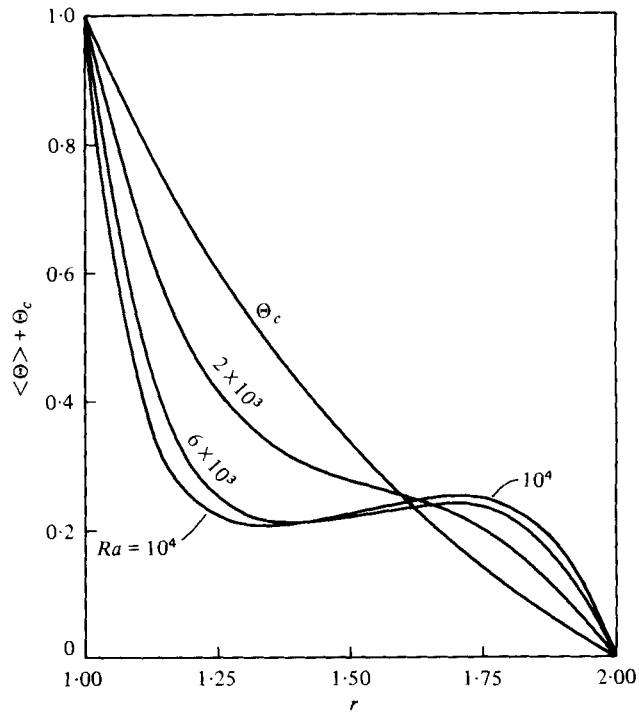

FIGURE 6. The spherically averaged temperature profile $\langle\Theta\rangle + \Theta_c$ for the even axisymmetric solutions with $N_r = 8$ and $N_\theta = 14$ at several different Rayleigh numbers. The conduction temperature profile Θ_c is also shown.

4.3. *Mean temperature profiles for the even solutions*

The spherically averaged temperature profile is $\Theta_c + \langle\Theta\rangle$. Using (2.4) and (2.13) we can write

$$\Theta_c + \langle\Theta\rangle = \frac{r_1 r_2}{r} - r_1 + \sum_{j=1}^{\infty} \bar{r}_{0j} \sin\lambda_j (r - r_1). \tag{4.6}$$

Figure 6 shows $\Theta_c + \langle\Theta\rangle$ *vs.* r at several values of Ra for the even solutions with $N_r = 8$ and $N_\theta = 14$. The basic state conduction temperature profile is also shown. Convection tends to produce a nearly uniform spherically averaged temperature, in the interior of the shell. At the higher values of Ra, the temperature drop across the outer thermal boundary layer is only about $\frac{1}{4}$ as large as the change in mean temperature across the inner boundary layer. Also, the inner thermal boundary layer is about as thick as the outer one. This is consistent with the constancy of total heat flow through the shell since the ratio of the inner to the outer surface areas is $\frac{1}{4}$. At $Ra = 6 \times 10^3$ and 10^4, the spherically averaged temperature actually increases with r in the interior of the shell. In a plane layer, the value of the nearly uniform interior mean temperature at high Ra is about 0·5; the much smaller value for the spherical shell is simply a consequence of the distribution of mass with radius in the spherical geometry (the volume-averaged value of Θ_c is only $\frac{2}{7}$, for example, when $\eta = 0{\cdot}5$). An estimate of this nearly uniform, steady, interior mean temperature $\langle\Theta_m\rangle$ can be derived by equating the heat transfer at the boundaries of the shell

$$r_1^2 \left(\frac{1 - \langle\Theta_m\rangle}{\delta_1} \right) = r_2^2 \frac{\langle\Theta_m\rangle}{\delta_2}, \tag{4.7}$$

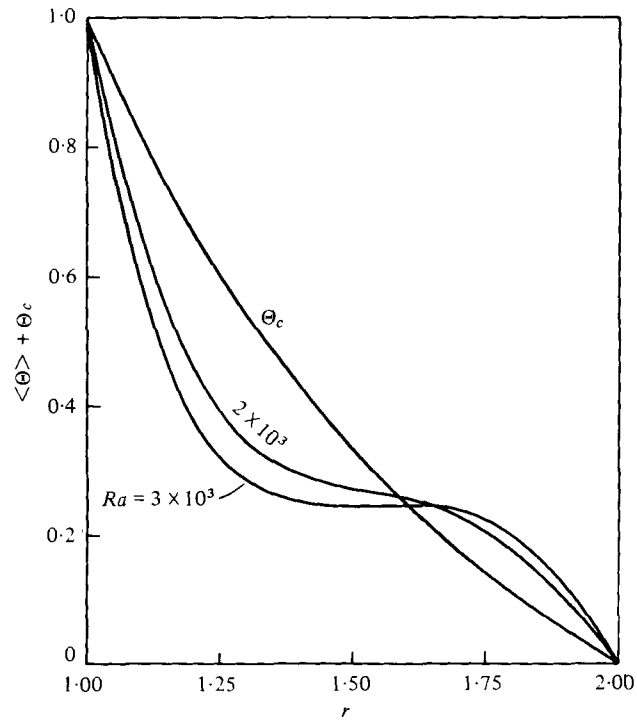

FIGURE 7. Same as figure 6 with $N_r = 8$ and $N_\theta = 9$.

where δ_1 and δ_2 denote the thicknesses of the thermal boundary layers which form at the inner and outer boundaries at high Rayleigh number. With $\delta_1 \approx \delta_2$ we find

$$\langle\Theta_m\rangle = \eta^2/(1+\eta^2), \tag{4.8}$$

which, for $\eta = 0{\cdot}5$, gives $\langle\Theta_m\rangle = 0{\cdot}2$, close to the value of about 0·22 shown in figure 6.

4.4. *Mean temperature profiles for the general solutions*

Figure 7 shows $\Theta_c + \langle\Theta\rangle$ *vs.* r at $Ra = 2000$ and 3000 for the general solutions with $N_r = 8$ and $N_\theta = 9$. These temperature profiles are quite similar to the ones obtained for the even solutions. Even at the relatively low value of $Ra = 3000$, the spherically averaged temperature in the interior of the shell is nearly uniform at about 0·24 and boundary layers of comparable thickness can be discerned at the inner and outer shell boundaries.

4.5. *Isotherms and streamlines for the even solutions*

Streamlines and isotherms in a meridional plane are shown in figure 8 for the even solutions with $N_r = 8$ and $N_\theta = 14$ at $Ra = 2000$, 6000 and 10000. Because of the symmetry of the solutions about the equatorial plane, only the range $0 \leqslant \theta \leqslant \frac{1}{2}\pi$ is shown. There is one fast cell and one slow one in each hemisphere. This indicates that the motion is dominated by the $l = 4$ mode. There is upwelling at the equator and at the poles. The fast cell adjacent to the equator grows in size as Ra increases while the slower, counter-rotating cell is confined more to the polar region. The distortion of the isotherms is as expected from the character of the streamlines.

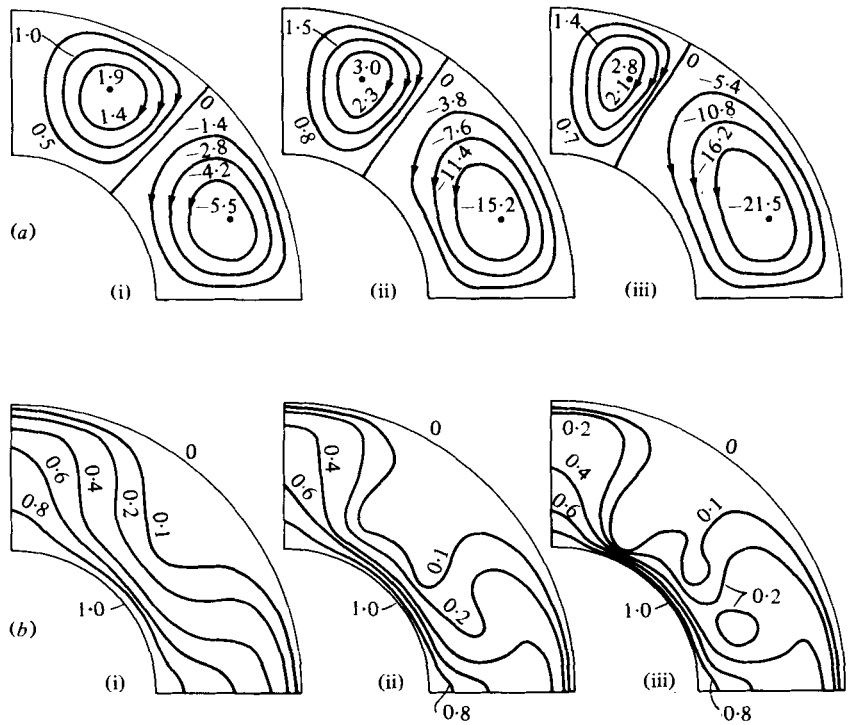

FIGURE 8. (*a*) Streamlines and (*b*) isotherms in a meridional plane for even axisymmetric solutions with $N_r = 8$ and $N_\theta = 14$. (i) $Ra = 2000$; (ii) $Ra = 6000$; (iii) $Ra = 10000$.

4.6. *Isotherms and streamlines for the general solutions*

Figure 9 shows the streamlines and isotherms in a meridional plane for the general solutions with $N_r = 8$ and $N_\theta = 9$ at $Ra = 2000$ and 3000. It is seen that the general solutions represent an $l = 3$ convective motion. The equatorial cell rotates more rapidly than do the polar cells. Upwelling occurs at one of the poles and at about 45° latitude in the opposite hemisphere. The asymmetry about the equator is particularly obvious in the isotherm patterns.

4.7. *Spectral content of* $\langle\Theta^2\rangle$, $\langle v_r^2\rangle$ $\langle v_\theta^2\rangle$: *even solutions*

The contributions of individual surface harmonics to the convective motions can be assessed by computing the spherically averaged kinetic energies $\langle v_r^2\rangle$ and $\langle v_\theta^2\rangle$ and the mean square temperature deviation $\langle\Theta^2\rangle$ from (2.8), (2.13) and (2.14). These quantities are given by

$$\langle v_r^2\rangle = \sum_{l=0}^{\infty} \langle v_r^2\rangle_l, \tag{4.9}$$

where

$$\langle v_r^2\rangle_l = \frac{1}{2}\left\{(1-\eta)\,Ra\,l(l+1)\sum_{j=1}^{\infty}\bar{\tau}_{lj}\frac{f_{lj}}{r}\right\}^2, \tag{4.10}$$

by

$$\langle v_\theta^2\rangle = \sum_{l=0}^{\infty} \langle v_\theta^2\rangle_l, \tag{4.11}$$

where

$$\langle v_\theta^2\rangle_l = \frac{1}{2}\left\{(1-\eta)\,Ra\,l(l+1)\sum_{j=1}^{\infty}\bar{\tau}_{lj}\frac{1}{r}\frac{d(rf_{lj})}{dr}\right\}^2, \tag{4.12}$$

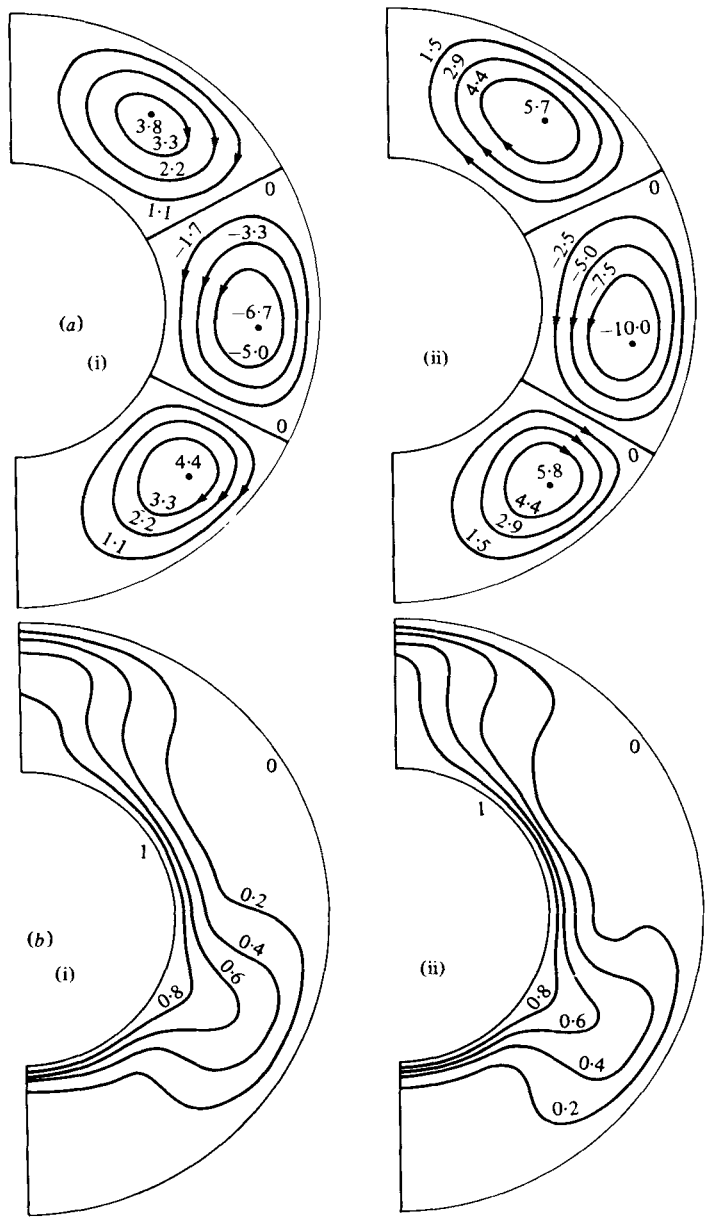

FIGURE 9. Same as figure 8 for the general axisymmetric solutions with $N_r = 8$ and $N_\theta = 9$. (i) $Ra = 2000$; (ii) $Ra = 3000$.

and by
$$\langle \Theta^2 \rangle = \sum_{l=0}^{\infty} \langle \Theta^2 \rangle_l, \tag{4.13}$$

where
$$\langle \Theta^2 \rangle_l = \left\{ \sum_{j=1}^{\infty} \bar{\tau}_{lj} \sin \lambda_j (r - r_1) \right\}^2. \tag{4.14}$$

Table 2 gives the spectral components $\langle v_r^2 \rangle_l$, $\langle v_\theta^2 \rangle_l$ and $\langle \Theta^2 \rangle_l$ for the even solution with $Ra = 3000$, $N_r = 8$, $N_\theta = 14$ at $r = 1{\cdot}2$, $1{\cdot}5$ and $1{\cdot}8$. The solution is strongly dominated

	$r = 1{\cdot}2$			$r = 1{\cdot}5$			$r = 1{\cdot}8$		
l	$\langle\Theta^2\rangle_l$	$\langle v_r^2\rangle_l$	$\langle v_\theta^2\rangle_l$	$\langle\Theta^2\rangle_l$	$\langle v_r^2\rangle_l$	$\langle v_\theta^2\rangle_l$	$\langle\Theta^2\rangle_l$	$\langle v_r^2\rangle_l$	$\langle v_\theta^2\rangle_l$
0	0·075	0·0	0·0	0·007	0·0	0·0	0·007	0·0	0·0
2	0·003	5·62	200·0	0·005	9·28	5·21	0·003	2·06	99·5
4	0·031	65·1	2359·0	0·024	114·0	108·0	0·017	27·8	1257
6	0·001	0·346	9·12	0·0	0·309	0·423	0·0	0·031	2·53
8	0·002	1·41	55·8	0·001	2·58	2·04	0·0	0·626	27·2
10	0·0	0·063	2·38	0·0	0·097	0·007	0·0	0·018	0·967
12	0·0	0·073	3·44	0·0	0·140	0·006	0·0	0·021	1·36
14	0·0	0·007	0·297	0·0	0·008	0·031	0·0	0·0	0·048
$\langle\Theta^2\rangle$		0·112			0·037			0·027	
$\langle v_\theta^2\rangle$		73·0			126·0			31·0	
$\langle v_r^2\rangle$		2630·0			116·0			1389·0	

TABLE 2. Spectral contributions to the mean square velocities $\langle v_r^2\rangle$, $\langle v_\theta^2\rangle$ and the mean square temperature deviation $\langle\Theta^2\rangle$ for the even solution at $Ra = 3000$, $Nr = 8$, $N_\theta = 14$.

by the $l = 4$ mode; the $l = 2$ mode is the next most important contributor to the flow. It is interesting that while the $l = 2$ mode has the minimum critical Rayleigh number for the even modes, the $l = 4$ mode dominates the finite amplitude solution at $Ra = 3000$.

4.8. *Spectral content of* $\langle\Theta^2\rangle$, $\langle v_r^2\rangle$, $\langle v_\theta^2\rangle$: *general solutions*

The spectral contributions of individual spherical harmonics to the general solutions for $Ra = 3000$ and $N_r = 8$, $N_\theta = 9$ are given in table 3. The dominant mode is clearly $l = 3$, which also has the minimum critical Rayleigh number for the onset of convection in the spherical shell. The $l = 6$ mode, which makes the next most important contribution to the flow, is undoubtedly generated by the nonlinear interaction of $l = 3$ with itself. The $l = 2$ and $l = 4$ modes make small, but non-negligible, contributions to this odd mode-dominated general solution.

5. The preferred axisymmetric steady solutions

In this section we consider the stability of the even axisymmetric steady solutions to a general axisymmetric perturbation. The even steady states satisfy [see equation (2.18)]

$$0 = \sum_{j=1}^{\infty} L_{ljk}\bar{\tau}_{lj} + \sum_{n,m=0,2,4}^{\infty}\sum_{l,j=1}^{\infty} N_{nmijlk}\bar{\tau}_{ni}\bar{\tau}_{mj}, \tag{5.1}$$

with $\bar{\tau}_{lj} = 0$ for l odd. A stability analysis can be carried out by substituting

$$\tau_{lj} = \bar{\tau}_{lj} + \tau'_{lj}$$

in (2.18), using (5.1) to simplify the result. One finds the linearized equations

$$\frac{d}{dt}\tau'_{lk} = \sum_{n=1,3,5}^{\infty}\sum_{i=1}^{\infty} E_{lkni}\tau'_{ni}, \quad l = 1, 3, 5, \ldots, \tag{5.2}$$

where

$$E_{lkni} = L_{lik}\delta_{ln} + \sum_{m=0,2,4}^{\infty}\sum_{j=1}^{\infty}\{N_{nmijlk} + N_{mnjilk}\}\bar{\tau}_{mj}. \tag{5.3}$$

The growth or decay rates of the perturbations are given by the eigenvalues σ of E_{lkni}. We have found the eigenvalue with the largest real part to be real. Figure 10 shows the maximum eigenvalue $\mathrm{Max}(\sigma)$ as a function of Ra for $N_r = 8$ and $N_\theta = 10$, 12, and 14. The determination of σ is seen to be sensitive to N_θ. For $Ra \lesssim 4400$ it is clear that $\sigma_{\max}$ is accurately determined for $N_\theta = 14$. Since $\sigma_{\max} > 0$, we conclude that the even solutions are unstable and that the general solutions represent the preferred steady axisymmetric convective motion for $Ra \lesssim 4400$. To determine the stability of even solutions at higher values of Ra would require a more accurate computation of the steady states.

6. Stability of the axisymmetric steady states to azimuthal perturbations

Linear stability theory (Chandrasekhar 1961) is capable of predicting Ra_{cr} and the number of cells in a meridional plane. However, the eigensolutions are degenerate and one cannot determine whether the motion is axisymmetric or non-axisymmetric.

	$r = 1{\cdot}2$			$r = 1{\cdot}5$			$r = 1{\cdot}8$		
l	$\langle\Theta^2\rangle_l$	$\langle v_r^2\rangle_l$	$\langle v_\theta^2\rangle_l$	$\langle\Theta^2\rangle_l$	$\langle v_r^2\rangle_l$	$\langle v_\theta^2\rangle_l$	$\langle\Theta^2\rangle_l$	$\langle v_r^2\rangle_l$	$\langle v_\theta^2\rangle_l$
0	0·081	0·0	0·0	0·008	0·0	0·0	0·007	0·0	0·0
1	0·001	0·512	18·0	0·003	0·825	0·355	0·001	0·176	8·73
2	0·0	0·637	23·8	0·0	0·140	1·027	0·0	0·273	12·5
3	0·033	66·3	2357	0·029	111	78·8	0·022	25·8	1207
4	0·0	0·935	33	0·0	1·49	0·486	0·0	0·30	15·8
5	0·0	0·004	0·142	0·0	0·005	0·0	0·0	0·001	0·036
6	0·003	3·8	142·0	0·002	6·78	6·25	0·001	1·67	73·4
7	0·002	0·683	18·9	0·0	0·714	0·114	0·0	0·115	6·42
8	0·0	0·0	0·109	0·0	0·012	0·196	0·0	0·005	0·209
9	0·001	0·523	19·5	0·0	0·794	0·025	0·0	0·141	7·62
$\langle\Theta^2\rangle$		0·121			0·042			0·031	
$\langle v_\theta^2\rangle$		73·0			122·0			28·0	
$\langle v_r^2\rangle$		2612·0			87·0			1332·0	

TABLE 3. Spectral contributions to $\langle v_r^2\rangle$, $\langle v_\theta^2\rangle$ and $\langle\Theta^2\rangle$ for the general solution at $Ra = 3000$, $Nr = 8$, $N_\theta = 9$.

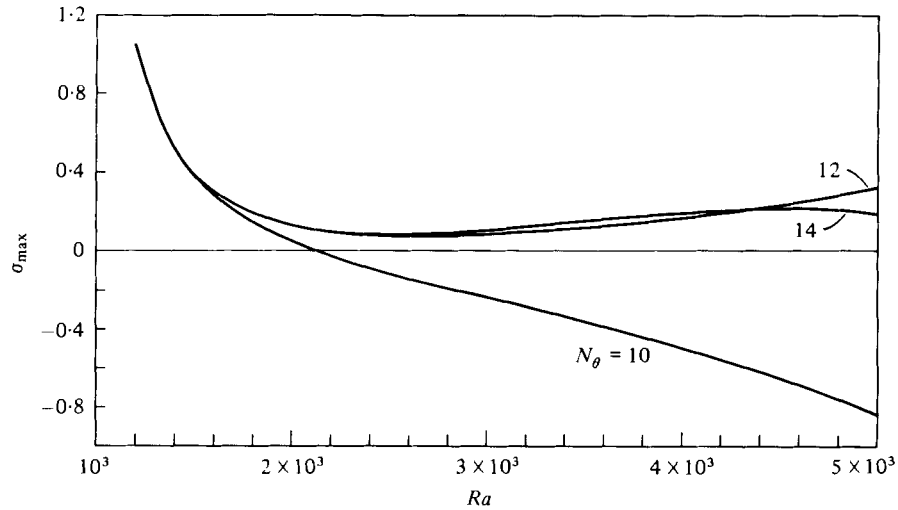

FIGURE 10. The maximum eigenvalue σ_{max} as a function of Ra for a linearized stability analysis of even axisymmetric steady states to general axisymmetric perturbations. σ positive indicates growth or instability. $N_r = 8$.

Busse (1975) has resolved the degeneracy of even axisymmetric solutions for slightly supercritical Ra. However, his results are not applicable in our case ($\eta = 0{\cdot}5$) since the minimum Ra_{cr} corresponds to an odd mode ($l = 3$) and we have already determined that the preferred axisymmetric steady states are the general solutions. Thus, we must still resolve the issue of the stability of the axisymmetric steady states, in particular the general solutions, to azimuthal perturbations.

We consider an infinitesimal three-dimensional perturbation (denoted by primes) superimposed on the steady axisymmetric solution $\bar{\Theta}$, $\bar{\Phi}$. By analogy with the forms of the expansions (2.13) and (2.14) for $\bar{\Theta}$ and $\bar{\Phi}$, the perturbations Θ' and Φ' are assumed to have the representations

$$\Theta' = \sum_{l=0}^{\infty}\sum_{j=1}^{\infty} \tau_{lj}'^{\beta}(t)\sqrt{2}\sin j\pi(r-r_1)\cos\beta\phi P_l^\beta(\cos\theta), \tag{6.1}$$

$$\Phi' = \sum_{l=0}^{\infty}\sum_{j=1}^{\infty} (1-\eta)\,Ra\,\tau_{lj}'^{\beta}(t)\,rf_{lj}(r)\cos\beta\phi P_l^\beta(\cos\theta), \tag{6.2}$$

where $\beta = 1, 2, \ldots, l$ and P_l^β are normalized Legendre functions

$$\int_{-1}^{1} P_l^\beta(\mu)\,P_m^\beta(\mu)\,d\mu = \delta_{lm}, \tag{6.3}$$

The differential equation for $\tau_{lj}'^{\beta}$ is obtained by substituting (2.13) and (2.14) for $\bar{\Theta}$, $\bar{\Phi}$ and (6.1) and (6.2) for Θ', Φ' into (2.3), linearizing the resulting expression, multiplying by $\sin j\pi(r-r_1)\cos\beta\phi P_l^\beta(\cos\theta)$ and integrating over the volume of the spherical shell. In carrying out the above one obtains the velocity from $\bar{\Phi}+\Phi'$ using (2.8); use is also made of the fact that $\bar{\tau}_{lj}$ satisfy (2.18) with $d\bar{\tau}_{lj}/dt = 0$. After considerable algebra one finds

$$\frac{d}{dt}\tau_{lk}'^{\beta} = \sum_{n=\beta}^{\infty}\sum_{i=1}^{\infty} F_{lkni}^{\beta}\tau_{ni}'^{\beta}, \quad l = \beta, \beta+1, \ldots \tag{6.4}$$

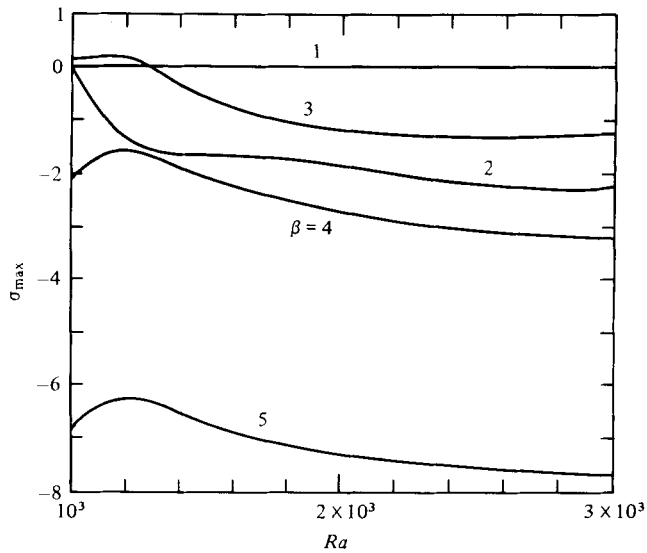

FIGURE 11. The largest value of σ as a function of Rayleigh number for azimuthal perturbations of the general axisymmetric solutions. β is the azimuthal wave number. $N_r = 8$ and $N_\theta = 9$. Positive σ indicates instability.

where

$$F^{\beta}_{lkni} = L_{lik}\,\delta_{ln} - (1-\eta)\,Ra \sum_{m=0}^{N_\theta} \sum_{j=1}^{N_r} \times \{m(m+1)\,C_{mjik} + n(n+1)\,C_{nijk} + [D_{mjik} + D_{nijk}]\,a_{mnl}\}\,G^{\beta}_{mln}\,\bar{\tau}_{mj}, \tag{6.5}$$

$$G^{\beta}_{mln} = \int_{-1}^{+1} P_m(x)\,P^{\beta}_n(x)\,P^{\beta}_l(x)\,dx, \tag{6.6}$$

and L_{lik}, C_{nijk}, D_{mjik}, a_{mnl} are given by (2.19), (2.23)–(2.25).

The eigenvalues of F^{β}_{lkni}, denoted by σ, represent either the growth or decay rates of the perturbation. We have found the eigenvalue with the largest real part to be real; thus the axisymmetric steady solutions are stable only if $\sigma_{\max} < 0$. Figure 11 shows $\sigma_{\max}$ as a function of Ra for the general solutions with $N_\theta = 9$ and $N_r = 8$. It is seen that perturbations with $\beta = 2$, 4 and 5 are decaying, while perturbations with $\beta = 1$ are neutral. Perturbations with $\beta = 3$ are growing for $Ra \lesssim 1280$ and decaying for $Ra \gtrsim 1280$. Thus, one concludes that while three-dimensional convection is preferred at the onset of convection, steady axisymmetric general solutions are stable for $Ra \gtrsim 1280$. While axisymmetric general solutions are stable for $Ra \gtrsim 1280$, they are not necessarily preferred over the non-axisymmetric solutions. For these Rayleigh numbers, axisymmetric general solutions and non-axisymmetric solutions may both be equally likely forms of steady convection, with only initial conditions determining which solution is realized.

The numerical calculations for the stability of the general axisymmetric solutions to azimuthal disturbances have shown that perturbations with $\beta = 1$ are neutral. This result can also be seen analytically as follows (F. Busse, personal communication).

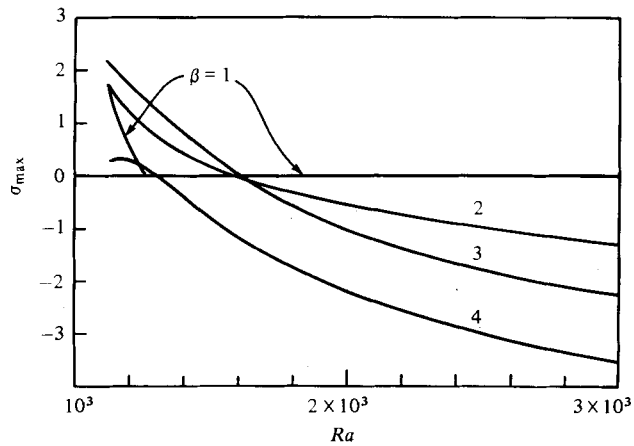

FIGURE 12. Same as figure 11 for the stability of even axisymmetric solutions to azimuthal perturbations. $N_r = 8$, $N_\theta = 12$.

Consider the expression for Θ resulting from the superposition of the general axisymmetric steady solution and a $\beta = 1$ perturbation,

$$\Theta = \sum_{l=0}^{\infty} \sum_{j=1}^{\infty} \sqrt{2} \sin \lambda_j (r - r_1) \{\bar{\tau}_{lj} P_l(\cos\theta) + \tau'^1_{lj} \cos\phi P_l^1(\cos\theta)\}. \tag{6.7}$$

With the aid of the addition theorem for Legendre functions (Smythe 1968, p. 165), we can rewrite (6.7) as

$$\Theta = \sum_{l=0}^{\infty} \sum_{j=1}^{\infty} \bar{\tau}_{lj} \sqrt{2} \sin \lambda_j (r - r_1) P_l(\cos\theta'), \tag{6.8}$$

where θ' is the co-latitude measured from the axis of a new co-ordinate system whose axis is inclined by the small angle ϵ,

$$\epsilon = \frac{\tau'^1_{lj}}{\bar{\tau}_{lj}} \{l(l+1)\}^{-\frac{1}{2}}, \tag{6.9}$$

with respect to the axis of the original (r, θ, ϕ) co-ordinate system. Equation (6.8) is correct only to $O(\epsilon)$. Thus, the perturbation coefficients $\tau'^1_{lj} = \epsilon \bar{\tau}_{lj} (l(l+1))^{\frac{1}{2}}$ represent a steady axisymmetric solution to the linearized equations in a frame of reference infinitesimally close to the original co-ordinate system. As a result, we can conclude that there exists an eigensolution for a $\beta = 1$ perturbation that corresponds to $\sigma = 0$. We have, in fact, verified numerically that the ratio $\tau'^1_{lj} / \{\bar{\tau}_{lj} (l(l+1))^{\frac{1}{2}}\}$ is constant for the neutral solutions with $\beta = 1$.

Figure 12 shows σ_{max} *vs.* Ra for the even, axisymmetric, steady solutions with $N_r = 8$ and $N_\theta = 12$. At the onset of convection, the growth of perturbations with $\beta = 1, 2, 3, 4$ shows that the preferred motion is fully three-dimensional. This is in agreement with Busse's (1975) results. However, the even solutions are stable to azimuthal perturbations for $Ra > 1800$. While there is a growing perturbation with $\beta = 1$ for slightly supercritical Ra ($\lesssim 1260$), we have also found the neutral solution for these values of Ra. The stability of the even solutions to azimuthal perturbations is of limited physical significance, since the even solutions are always unstable to the general ones.

7. Summary

We have carried out numerical calculations of axisymmetric convective motions in a spherical shell heated from below with $\eta = 0{\cdot}5$. For a given Rayleigh number, there exists either a 4-cell equatorially symmetric solution or a 3-cell general solution. The even axisymmetric solutions have been studied for Ra as large as about 10 times the critical value, while the general, axisymmetric solutions have been investigated only for Ra up to about 3 times the critical value. A linear stability analysis indicates that the preferred axisymmetric convection includes contributions from both even and odd Legendre functions, i.e. the equatorially symmetric motions are unstable to general axisymmetric perturbations. A linearized stability analysis of the axisymmetric solutions to azimuthal perturbations shows that fully three-dimensional motions are to be expected at the onset of convection; however, axisymmetric convection is stable, though not necessarily preferred for $Ra \gtrsim 1280$. The present study has been limited to isothermal, stress-free boundaries with no internal heating. Extensions to other boundary conditions (e.g. adiabatic lower boundary) with internal heating are in progress.

This research was supported by the Planetology Program, Office of Space Science, N.A.S.A. grant NGR 05-007-317, by NSF grant EAR 77-15198 and by the Aerospace Sponsored Research Program. Computing funds were contributed by the University of California, Los Angeles and by Rutgers University. We thank F. H. Busse for helpful discussions.

Appendix

A general representation of the solenoidal velocity field is

$$\mathbf{v} = \left(0, \frac{1}{r\sin\theta}\frac{\partial\chi}{\partial\phi}, -\frac{1}{r}\frac{\partial\chi}{\partial\theta}\right) + \text{poloidal part given in (2.8)}, \tag{A 1}$$

where χ represents the toroidal part of $\mathbf{v}$ (Chandrasekhar 1961). From the equation of motion (2.2), it is straightforward to conclude that

$$\nabla^2 L^2(\chi/r) = 0. \tag{A 2}$$

Since χ/r satisfies (A 2) it is also a solution of Laplace's equation (this is true for all the spherical harmonic components of χ/r except perhaps for the $l = 0$ term which does not contribute to $\mathbf{v}$ anyway). Thus $(\chi/r) \equiv 0$ since $\nabla^2(\chi/r) = 0$ and χ/r satisfies homogeneous boundary conditions on the inner and outer surfaces of the spherical shell.

REFERENCES

Busse, F. H. 1967 On the stability of two-dimensional convection in a layer heated from below. *J. Math. Phys.* **46**, 140–150.

Busse, F. H. 1975 Patterns of convection in spherical shells. *J. Fluid Mech.* **72**, 67–85.

Cassen, P. & Young, R. E. 1975 On the cooling of the Moon by solid convection, *The Moon* **12**, 361–368.

Chandrasekhar, S. 1961 *Hydrodynamic and Hydromagnetic Stability*, cha. II and VI. Clarendon.

Clever, R. M. & Busse, F. H. 1974 Transition to time-dependent convection. *J. Fluid Mech.* **65**, 625–645.

DAVIS, P. J. & POLONSKY, I. 1964 Numerical interpolation, differentiation, and integration. In *Handbook of Mathematical Functions* (ed. M. Abramowitz & I. A. Stegun), pp. 875–924. Washington: National Bureau of Standards.

HSUI, A. T., TURCOTTE, D. L. & TORRANCE, K. E. 1972 Finite amplitude thermal convection within a self-gravitating fluid sphere. *Geophys. Fluid Dyn.* **3**, 35–44.

OXBURGH, E. R. & TURCOTTE, D. L. 1978 Mechanisms of continental drift. *Rep. Prog. Phys.* **41**, 1249–1312.

RICHTER, F. M. 1978 Mantle convection models. *Ann Rev. Earth Planet. Sci.* **6**, 9–19.

SCHUBERT, G. 1979 Subsolidus convection in the mantles of terrestrial planets. *Ann. Rev. Earth Planet. Sci.* **7**, 289–342.

SCHUBERT, G. & YOUNG, R. E. 1976 Cooling the Earth by whole mantle subsolidus convection: A constraint on the viscosity of the lower mantle. *Tectonophys.* **35**, 201–214.

SCHUBERT, G., YOUNG, R. E. & CASSEN, P. 1977 Solid state convection models of the lunar internal temperature. *Phil. Trans. Roy. Soc.* A **285**, 523–536.

SMYTHE, W. R. 1968 *Static and Dynamic Electricity*, 3rd edn. McGraw-Hill.

TOZER, D. C. 1967 Towards a theory of thermal convection in the mantle. In *The Earth's Mantle* (ed. T. F. Gaskell), pp. 325–353.

TURCOTTE, D. L., HSUI, A. T., TORRANCE, K. E. & OXBURGH, E. R. 1972 Thermal structure of the Moon. *J. Geophys. Res.* **77**, 6931–6939.

TURCOTTE, D. L. & OXBURGH, E. R. 1972 Mantle convection and the new global tectonics. *Ann. Rev. Fluid Mech.* **4**, 33–68.

YOUNG, R. E. 1974 Finite-amplitude thermal convection in a spherical shell. *J. Fluid Mech.* **63**, 695–721.

YOUNG, R. E. & SCHUBERT, G. 1974 Temperatures inside Mars: Is the core liquid or solid? *Geophys. Res. Lett.* **1**, 157–160.